ADVANCED ENERGY MATERIALS

Supporting Information

for *Adv. Energy Mater.*, DOI 10.1002/aenm.202501286

Selective Electrochemical Reduction of CO_2 to Metal Oxalates in Nonaqueous Solutions Using Trace Metal Pb on Carbon Supports Enhanced by a Tailored Microenvironment

Rowan S. Brower, Brian Wuille Bille, Shawn Chiu, Joseph T. Perryman, Libo Yao, Faridat O. Agboola, Cocoro A. Nagasaka, Yinuo Xie, Richard Gomez-Caballero, Ankita Kumari, Elizabeth K. Neumann, Anastassia N. Alexandrova, Charles C. L. McCrory* and Jesus M. Velázquez**

Selective Electrochemical Reduction of CO_2 to Metal Oxalates in Non-Aqueous Solutions using Trace Metal Pb on Carbon Supports Enhanced by a Tailored Microenvironment.

R. S. Brower[1], B. Wuille Bille[1], S. Chiu[2], J.T. Perryman[1], L. Yao[3], F. Agboola[4], C. A. Nagasaka[1], Y. Xie[1], R. Gomez[5], A. Kumari[1], E. Neumann[1],A. N. Alexandrova[2], C. C. L. McCrory[4,6*], J.M.Velázquez[1*]

[1]University of California-Davis, Department of Chemistry, Davis, CA

[2]University of California-Los Angeles, Department of Chemistry and Biochemistry, Los Angeles, CA

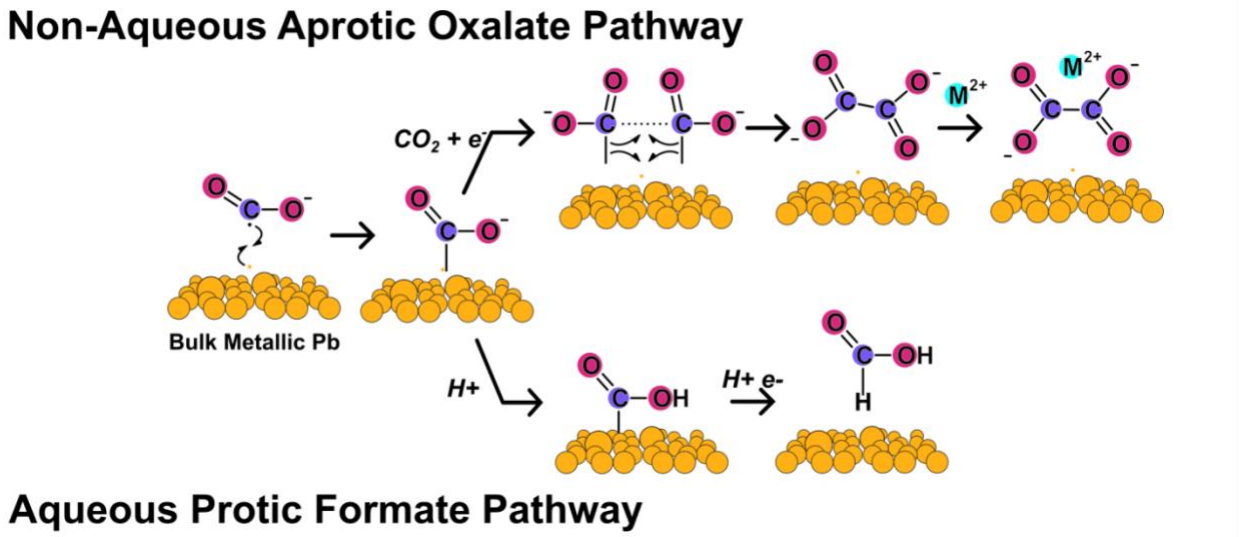
[3]University of Michigan, Department of Chemical Engineering, Ann Arbor, MI

[4]University of Michigan, Department of Chemistry, Ann Arbor, MI

[5]Universidad de Puerto Rico Recinto de Río Piedras, Department of Chemistry, San Juan, PR 00925-253

[6]University of Michigan, Macromolecular Science & Engineering Program, Ann Arbor, MI.

Oxalate vs. Formate Pathway on Bulk Metallic Pb

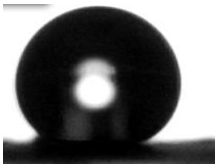
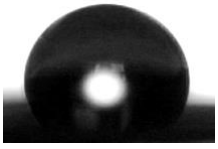
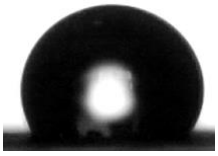
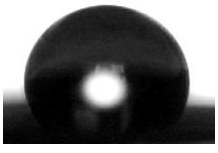


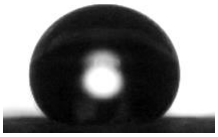
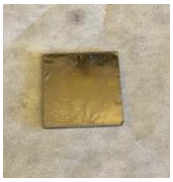
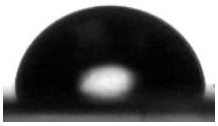
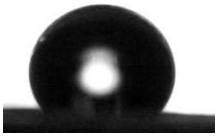
Scheme S1. CO_2 pathways on bulk metallic Pb in non-aqueous aprotic and aqueous protic media.

Table S1. Pb loading of each working electrode.

Working Electrodes	**Pb Loading (10^2 ng)**
TP	7.9 ± 2.2
TP-PTFE	6.4 ± 1.6
CP	1.5 ± 1.3
CP-PTFE	1.5 ± 1.4
GC	1.5 ± 1.1
GC-PTFE	1.2 ± 0.8
PG	0.4 ± 0.2
PG-PTFE	0.2 ± 0.3

Table S2. Descriptions and photos of sample electrodes used in this study.

Working Electrodes	Description	Photograph of Representative Electrode	Water Contact Angle[1] (WCA)	Contact Angle in 0.1 M nBu$_4$PF$_6$ in MeCN[1] (ECA)
TP (Toray Paper)	Toray Paper (060) was purchased from the Fuel Cell Store. It is a carbon fiber composite paper with a layer of PTFE (5 wt%).		θ = 137.0 ± 0.2° 	θ = 41.4 ± 1.6° 
TP-PTFE (Toray Paper with PTFE)	Toray Paper (060) was purchased from the Fuel Cell Store. It is a carbon fiber composite paper with a layer of PTFE (5 wt%). An additional 400 μl of PTFE ink was spray deposited onto this electrode.		θ = 99.5 ± 0.2° 	θ = 24.9 ± 0.9° 
CP (Carbon Paper)	Carbon paper was purchased from Fuel Cell Earth and has the same thickness as the toray paper electrodes, but without the PTFE treatment.		θ = 119.0 ± 0.3° 	0* Unable to measure contact angle due to solution uptake
CP (Carbon Paper with PTFE)	Carbon paper was purchased from Fuel Cell Earth and has the same thickness as the toray paper electrodes. 400 μl of ink was spray deposited onto this electrode.		θ = 98.2 ± 0.7° 	0* Unable to measure contact angle due to solution uptake

GC (Glassy Carbon)	Glassy Carbon was purchased from SPI supplies (Lot#1270526). It is a non-graphitizing carbon that combines ceramic properties with graphite properties.		θ = 20.1 ± 0.1° 	θ = 27.3 ± 1.0° 
GC-PTFE (Glassy Carbon with PTFE)	Glassy Carbon was purchased from SPI supplies. It is a non-graphitizing carbon that combines ceramic properties with graphite properties. 400 μl of ink was spray deposited onto this electrode.		θ = 130.5 ± 0.2° 	θ = 31.1 ± 1.1° 
PG (PG)	Highly Oriented Pyrolytic Graphite was purchased from SPI supplies. It is an ordered form of synthetic graphite.		θ = 92.7 ± 0.1° 	θ = 37.6 ± 1.0° 
PG (PG with PTFE)	Highly Oriented Pyrolytic Graphite was purchased from SPI supplies. It is an ordered form of synthetic graphite. 400 μl of ink was spray deposited onto this electrode.		θ = 123.0 ± 0.1° 	θ = 36.8 ± 1.3° 

[1]All reported contact angle measurements are averages from at least three measurements on each electrode, and the reported errors represent standard deviations. The droplet images shown are representative images used for contact angle determination on the electrode surface.

Electrochemical Cell Design

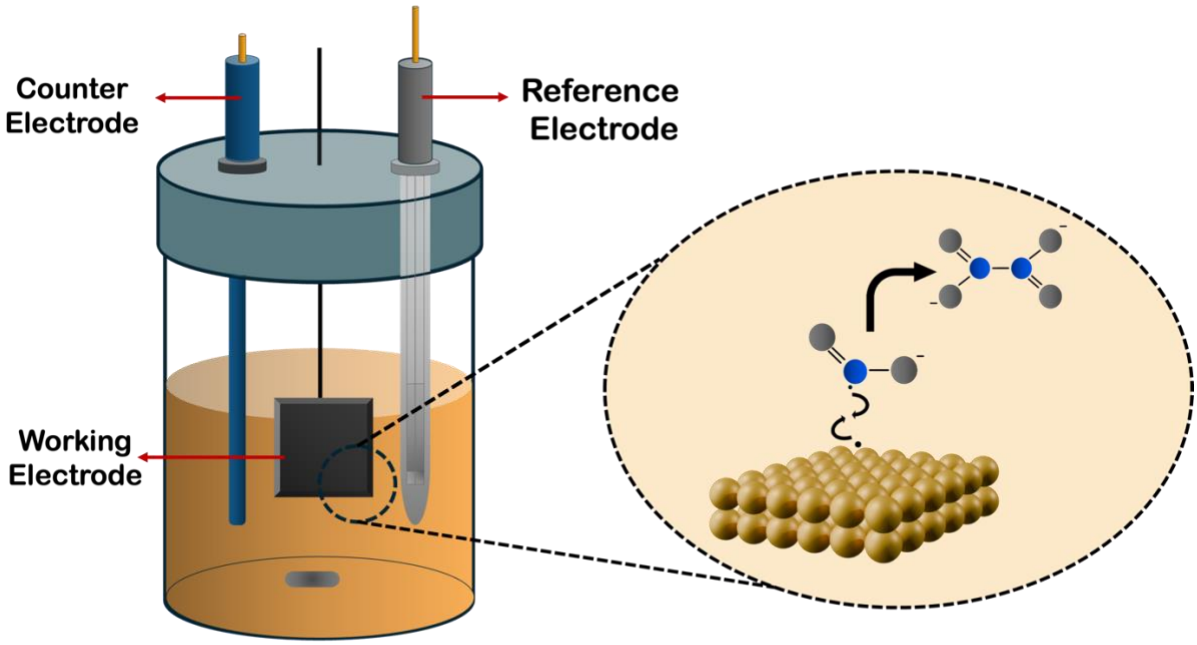


Figure S1. Cell diagram with a CBS working electrode (WE), Ag/AgCl reference electrode (RE), and sacrificial metal anode (CE).

Converting Potentials from Ag/AgCl to Fc/Fc+

Process for Converting Ag/AgCl Potentials to Fc/Fc+

Real/Applied Voltage in Cell Calculation

There is a 15% uncompensated resistance that is not accounted by the potentiostat. The real voltage is calculated using the formula below.

$$V_{real} = V_{applied} - [(0.15 * R_u) * I] \qquad \textbf{Eq.S1}$$

Where V_{real} is the real voltage in the cell

$V_{applied}$= the voltage applied with the instrument

R_u=Uncompensated Resistance (ohms)

I= Median Current Passed in Cell (Amps)

Fc/Fc+. The 0.56V value was obtained by completing an experiment where the redox couple was tested vs. Ag/AgCl as shown in figure S1.

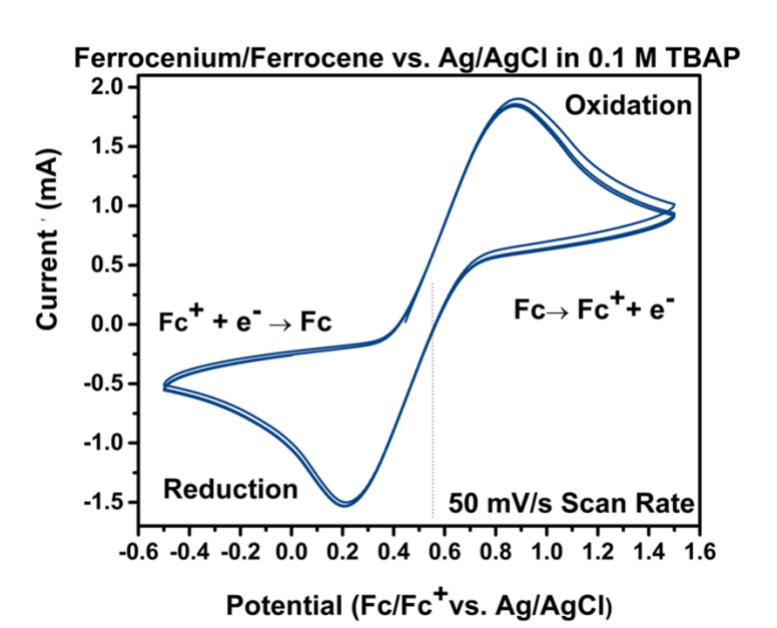


Figure S2. Cyclic voltammogram of Fc/Fc+ redox couple compared to Ag/AgCl in 0.1 M TBAP

Unlike aqueous systems, where the standard hydrogen electrode (SHE) provides a consistent reference, non-aqueous media lack a universal reference electrode due to variations in solvent properties and supporting electrolytes. The ferrocene/ferrocenium (Fc/Fc^+) redox couple offers a convenient alternative for nonaqueous electrolytes because it has well-defined, reversible one-electron transfer in organic solvents that is relatively similar across different solvent systems.[1, 2ref]

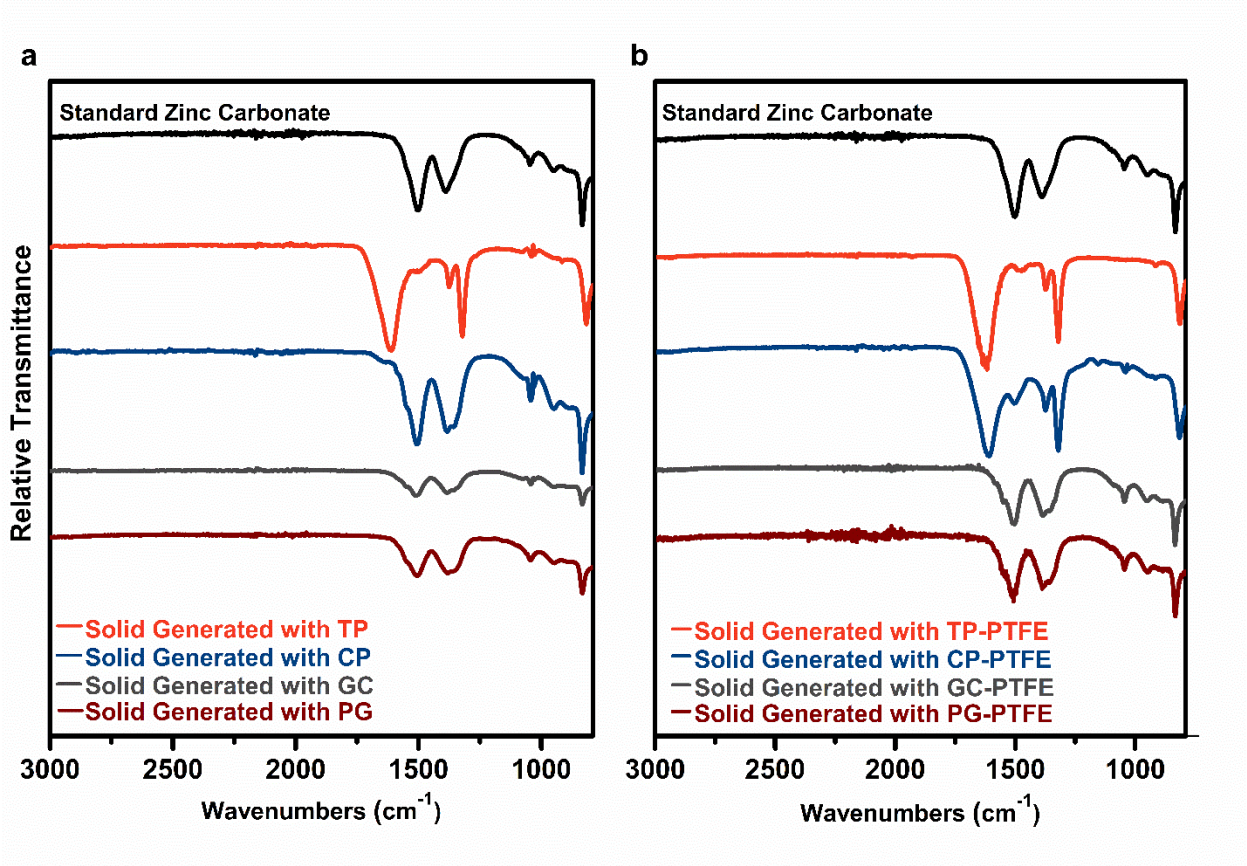
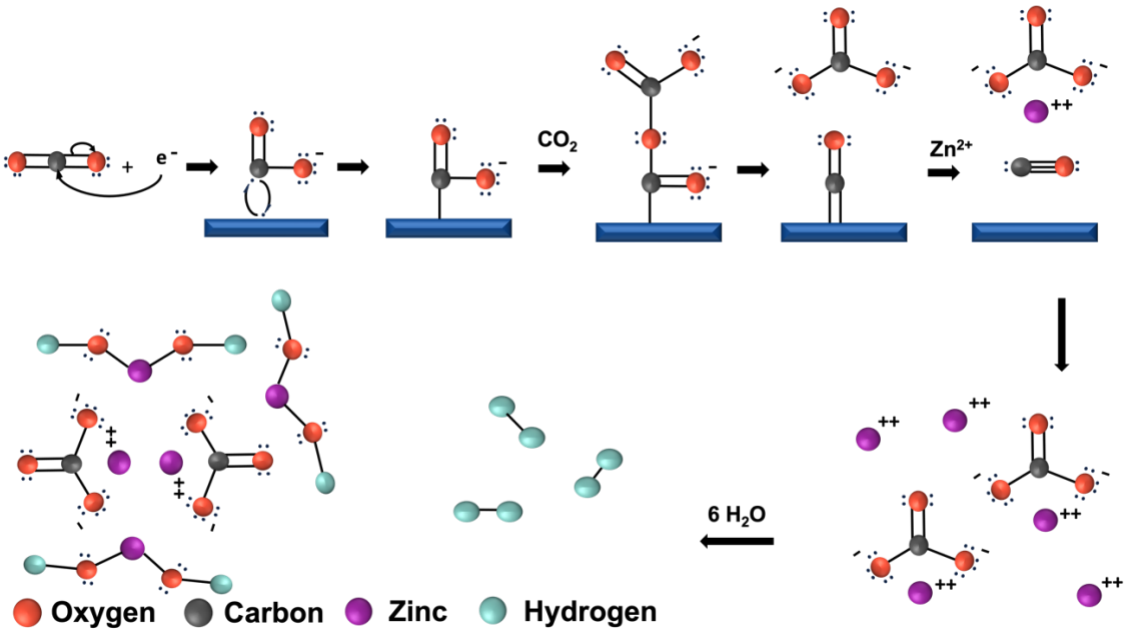


Figure S3. ATR-FTIR spectrum of working electrodes generated in CO_2 compared to Zinc Carbonate Basic.

Production of Zinc Carbonate Basic



Scheme S2. Reaction within the cell where CO and $ZnCO_3$ are produced.

Solid removal process involves washing the solid/solvent with ethanol and water.

Reaction Between Recovered Solid and Water

1. $2ZnCO_3(s) + 6H_2O(l) + 3Zn^{2+}(soln) \rightarrow 3H_2(g) + [ZnCO_3]_2*[Zn(OH)_2]_3\,(s)$

Quantification of Experimentally Generated Mass for Zinc Carbonate

The faradaic efficiency of generated Zinc Carbonate on E.Type 3 was calculated after gravimetric analysis of the generated solid. The solid was verified to have no zinc oxalate by dissolving the solid in ammonium hydroxide and running ^{13}C NMR where no oxalate peak was found. To get mass of experimentally generated $ZnCO_3$ the mass of the generated solid was multiplied by 0.228 which is equal to the mass ratio of 1 $ZnCO_3$ in Zinc Carbonate Basic (See EqS2) . The experimental mass was then used to calculate experimental mols which was then used with Eq. 1 to calculate FE_{ZnCO3}.

$Exp\ Mass_{Zinc\ Carbonate\ Basic}*0.228 = Exp\ Mass_{ZnCO3}$

Stability

To further evaluate catalyst stability, we monitored the current over time during each constant potential electrolysis (CPE) experiment. Figure S4 shows representative current–time data for the CP-PTFE electrode, which demonstrates relatively stable current density over the 5–8-hour electrolysis period during which 100 C of charge was passed. This stability supports the conclusion that the catalyst maintains consistent performance under the conditions tested. However, beyond this point, we observed visible accumulation of solid products on the electrode surface, which introduced mass transport limitations and contributed to increased cell resistance in preliminary extended experiments. These limitations underscore the need for future modifications to the cell design—such as improved product removal or flow cell configurations—to enable long-term electrolysis. Thus, while this study focuses on short-term catalytic behavior, it provides a basis for future investigations aimed at enhancing the durability and operational stability of the system.

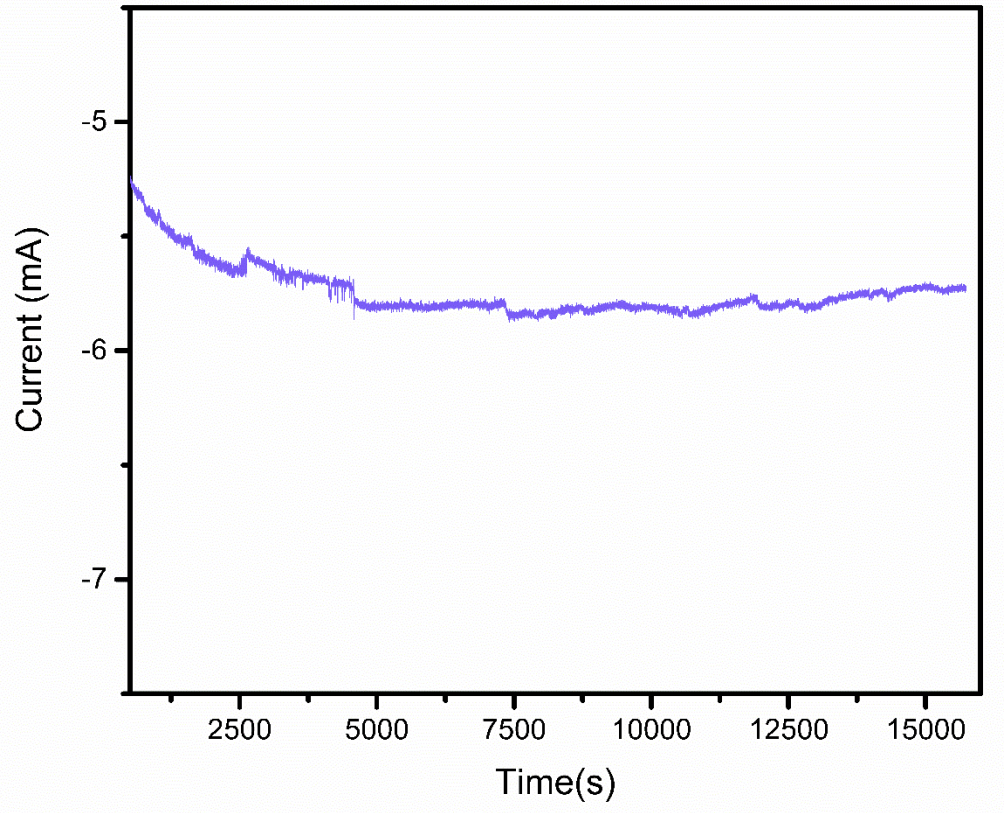


Figure S4. Current vs. time of CP-PTFE at -1.9V.

Product Analysis

Gaseous

For the detection of gas-phase products such as H_2 and CO, gas chromatography with thermal conductivity detection (GC–TCD) was implemented as is illustrated in Figure S4 using methods modified from literature[x], with a Thermo-Fisher GC equipped with a Carboxen® 1010 Porous Layer Open Tubular (PLOT) fused silica column (30m x 0.53mm x 10µm), with helium as a reference and carrier gas. Faradaic efficiencies for gas-phase products were calculated according to Eq.S3

$$FE(\%)=\frac{nFXV_i}{V_m Q_{tot}} \quad \textbf{(Eq.3)}$$

where n = # of electrons transferred per product molecule
F = Faraday's constant
X = Mole fraction of product gas in cell headspace
V_i = Volume of headspace injected
V_m = Molar volume of gas at ambient conditions
Q_{tot} = Total charge passed

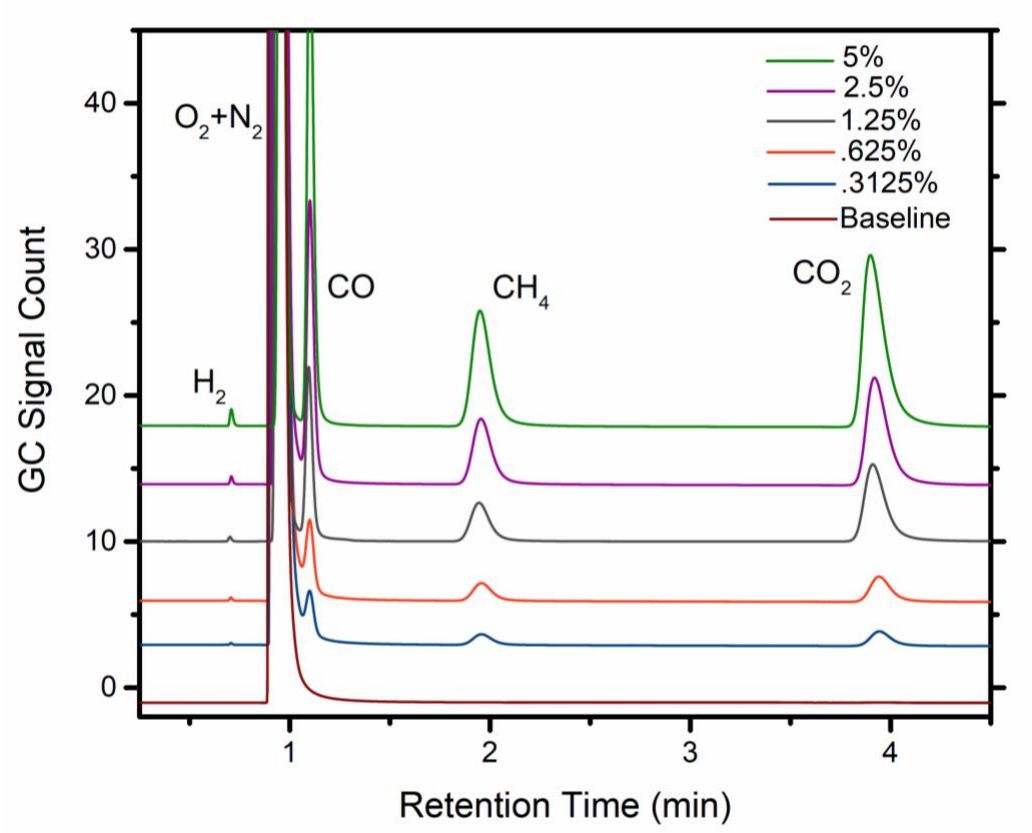


Figure S5. GC-TCD chromatograph illustrating the test injections used for calibration of H_2, CO, CO_2, and CH_4.

Liquid

To detect potential liquid products electrolytes aliquots were analyzed using a 400 MHz Bruker NMR spectrometer using pre-defined ^{1}H and ^{13}C programs with a TMS internal standard and $(CD_3)_2CO$ (see Figure S6 for a full NMR spectra). Any liquid products were below detection limits.

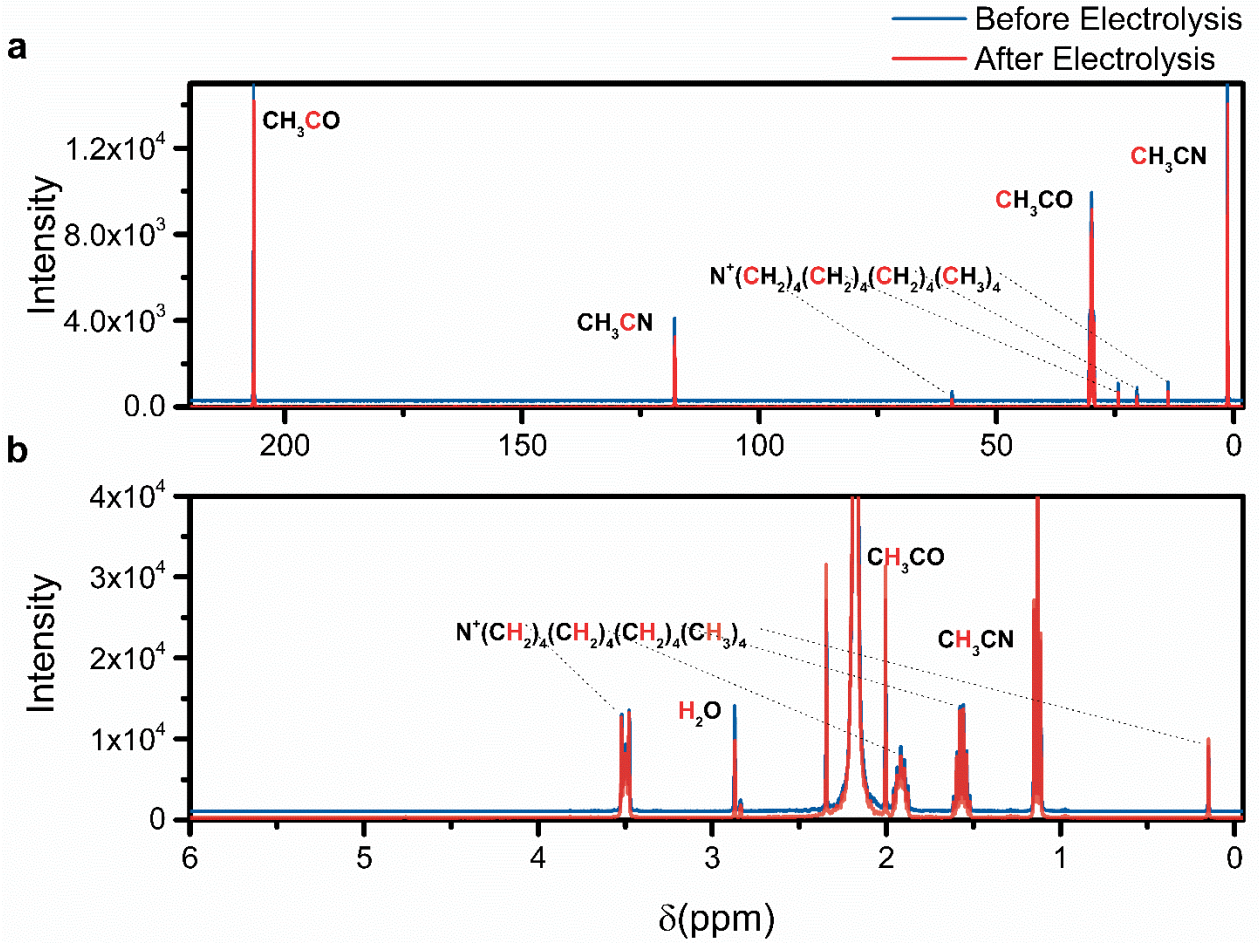


Figure S6. Complete ^{1}H NMR spectrum before and after electrolysis (a.). Complete ^{13}C NMR spectrum before and after electrolysis (b.).

Current Density Calculations

Current density (J) was calculated using equation sx.

$$J = \frac{I}{A}$$

Eq.S3

where,

I= the current in the cell (mA)

A= area of the electrode (cm^2)

Table S3. Faradaic efficiency values for TP and TP-PTFE electrodes at varying potentials

Potential	**Working Electrode**	**ZnC_2O_4**	**CO**	**H_2**
-2.1	**TP**	75.5 ± 7.5	2.8 ± 1.8	2.7 ± 2.3
-2.1	**TP-PTFE**	78.2 ± 5.1	1.8 ± 1.1	1.4 ± 0.4
-1.9	**TP**	75.5 ± 0.8	13.3 ± 9.2	0.7 ± 0.6
-1.9	**TP-PTFE**	82.0 ± 5.8	2.0 ± 0.3	2.5 ± 0.3
-1.8	**TP**	59.3 ± 8.9	14.7 ± 12.0	1.9 ± 1.2
-1.8	**TP-PTFE**	78.2 ± 3.5	3.0 ± 1.1	3.1 ± 0.8

Table S4. Faradaic efficiency values for TP,TP-PTFE, CP, and CP-PTFE electrodes at -1.9 V vs. Fc/Fc+

-1.9 V vs Fc/Fc+	**ZnC_2O_4**	**CO**	**H_2**	**$ZnCO_3$**
TP	75.5 ± 0.8	13.3 ± 9.2	0.7 ± 0.6	-[a]
TP-PTFE	82.0 ± 5.8	2.0 ± 0.3	2.5 ± 0.8	-[a]
CP	-[a]	79.2 ± 2.2	-[a]	16.8 ± 0.5
CP-PTFE	78.3 ± 3.5	7.3 ± 2.6	-[a]	-[a]
Bulk Pb	89.5 ± 4.2	1.2 ± 0.7	-[a]	-[a]

[a]Not detected at the limit of quantification (>0.1 wt%) of our measurement.

PTFE Loadings

To investigate the effect of PTFE loading on catalyst performance and microenvironment tuning for enhanced $C_2O_4^{2-}$ production, we evaluated three PTFE loadings on carbon paper (CP): 0 mg/cm² (uncoated), 9.4 mg/cm² (mass amount used on electrode PTFE analogs throughout the work), and 18.8 mg/cm². As shown in Figure S7, linear sweep voltammetry (LSV) data revealed that increasing PTFE content beyond 9.4 mg/cm² resulted in reduced current densities, indicating hindered charge transfer and mass transport. Faradaic efficiencies (FE) and partial current densities for oxalate production are shown in Figure S8. While the 18.8 mg/cm² PTFE loading yielded a slightly higher oxalate FE compared to 9.4 mg/cm², this came at the expense of overall current density, leading to lower total oxalate production rates. These findings suggest that excessive PTFE coverage may obstruct access to catalytically active Pb sites or reduce electrolyte penetration. Therefore, the 9.4 mg/cm² PTFE loading was identified as the optimal condition, offering a favorable balance between oxalate selectivity and electrochemical performance. This optimization highlights the importance of fine-tuning polymer content to engineer the catalyst microenvironment effectively.

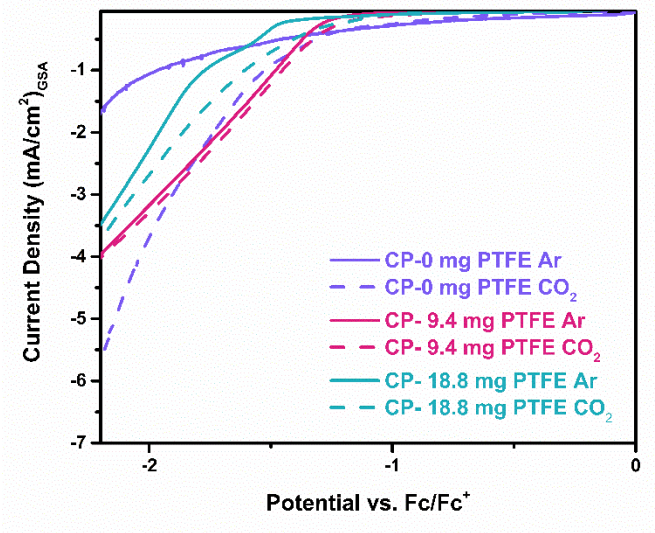


Figure S7. LSVs of CP with different mass loadings of PTFE in Ar and CO_2.

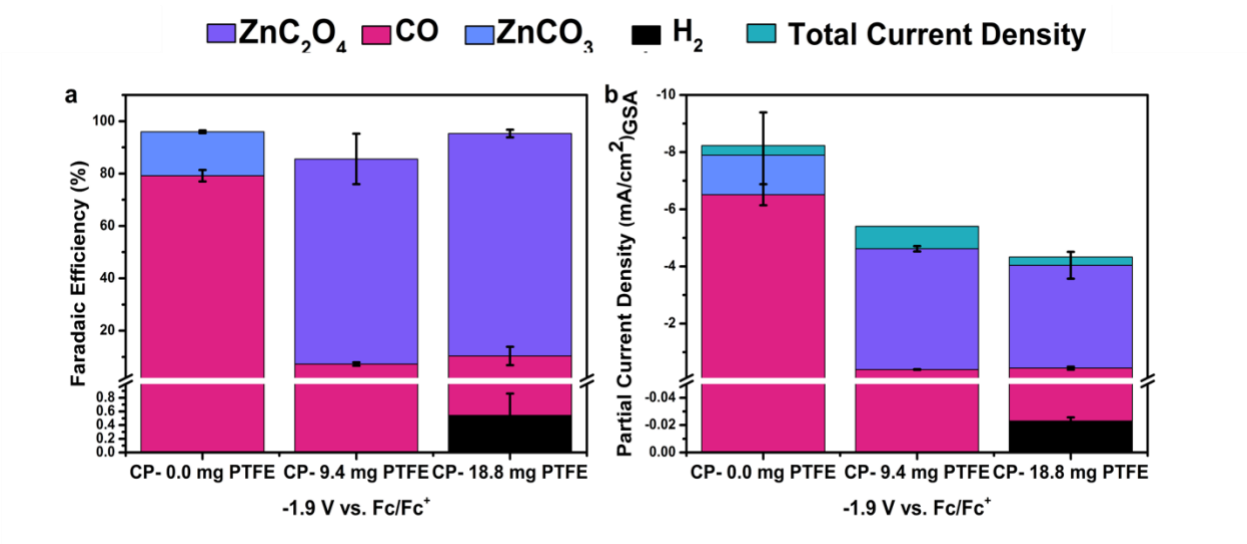


Figure S8. Full product distribution and partial current densities of various PTFE loadings on CP.

TOF

Assumptions

- All Pb content contained in the working electrodes and Pb plate were assumed to be active.
- The Pb plate used in this experiment was 0.5 g and was tested under the same conditions as the E.Types.
- TOF was calculated in molecules per second per active site.

Table S5. Values obtained from experimental results of TP, TP-PTFE, CP-PTFE and a Pb Standard at -1.9 V vs. Fc/Fc+ for 100 C.

	Mols of ZnC_2O_4	**Time of Exp (s)**	**Mols of Pb on Electrode**	**TOF (s^{-1})**	**Mass Activity mA/gPb**
TP	4.26×10^{-4}	15504	7.9×10^{-7}	7.2	29812
TP-PTFE	4.26×10^{-4}	17385	6.4×10^{-7}	7.9	34236
CP-PTFE	3.86×10^{-4}	13371	1.5×10^{-7}	38.8	136100
Bulk Pb Standard	4.64×10^{-4}	14505	2.4×10^{-3}	0.0028	10.6

Measuring CO_2R activity at different Pb loadings

Table S6. Faradaic efficiencies for products at different Pb loadings.

-1.9 V vs Fc/Fc+	**ZnC_2O_4**	**CO**	**H_2**	**$ZnCO_3$**
10 mg-CP	75.3 ± 1.3	5.9 ± 0.7	0.6 ± 0.6	-[a]
10 mg-CP PTFE	83.8 ± 6.2	5.3 ± 1.2	1.0 ± 0.0	-[a]
1 mg-CP	73.4 ± 8.7	9.5 ± 8.8	1.7 ± 0.2	-[a]
1 mg-CP-PTFE	79.7 ± 1.4	3.8 ± 1.0	0.3 ± 0.1	-[a]
0.1 mg-CP	72.1 ± 0.8	10.8 ± 5.0	1.6 ± 0.13	-[a]
0.1 mg-CP-PTFE	81.7 ± 3.2	4.1 ± 1.3	0.87 ± 0.48	-[a]
0.01 mg-CP	37.4 ± 1.2	35.4 ± 31.6	0.73 ± 0.64	11.2 ± 0.89
0.01 mg-CP-PTFE	71.7 ± 0.17	3.2 ± 2.7	2.01 ± 0.43	-[a]
0.0 mg-CP	-[a]	80.6 ± 1.1	-[a]	14.9 ± 0.23
0.0 mg-CP PTFE	-[a]	76.3 ± 8.8	-[a]	18.8 ± 1.9

[a]Not detected at the limit of quantification (0.1 wt%)of our measurement.

Computational

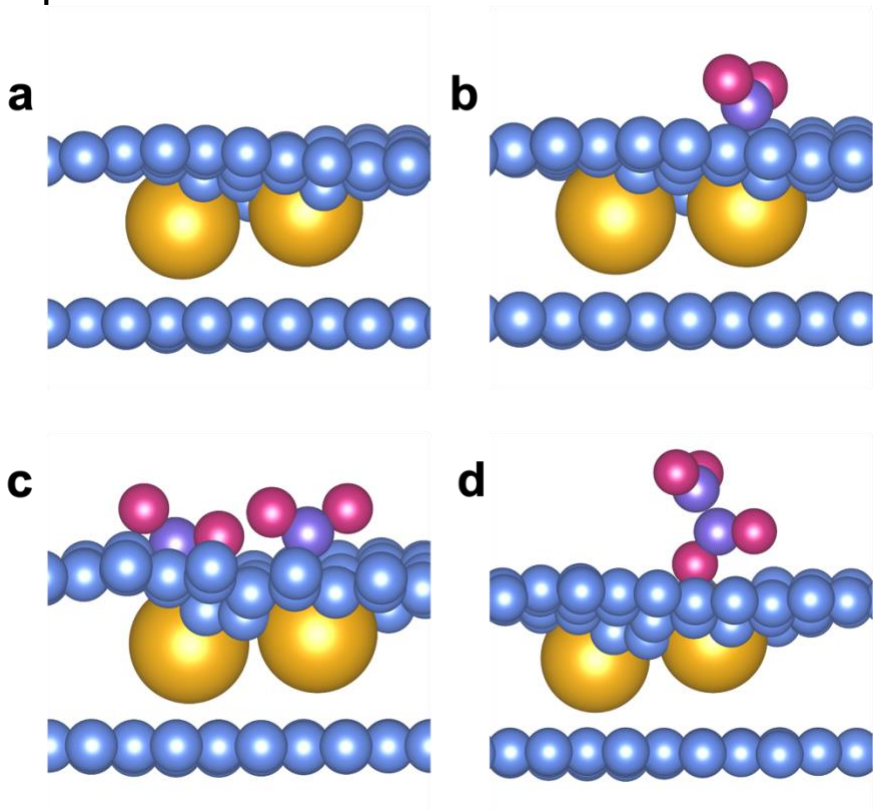


Figure S9. Side view of the optimized structures of (a) the bare surface, (b) $*CO_2^-$, (c) 2 $*CO_2^-$, and (d) $*C_2O_4^{2-}$.

Electrochemical Synthesis of Alternative Metal Oxalate Salts

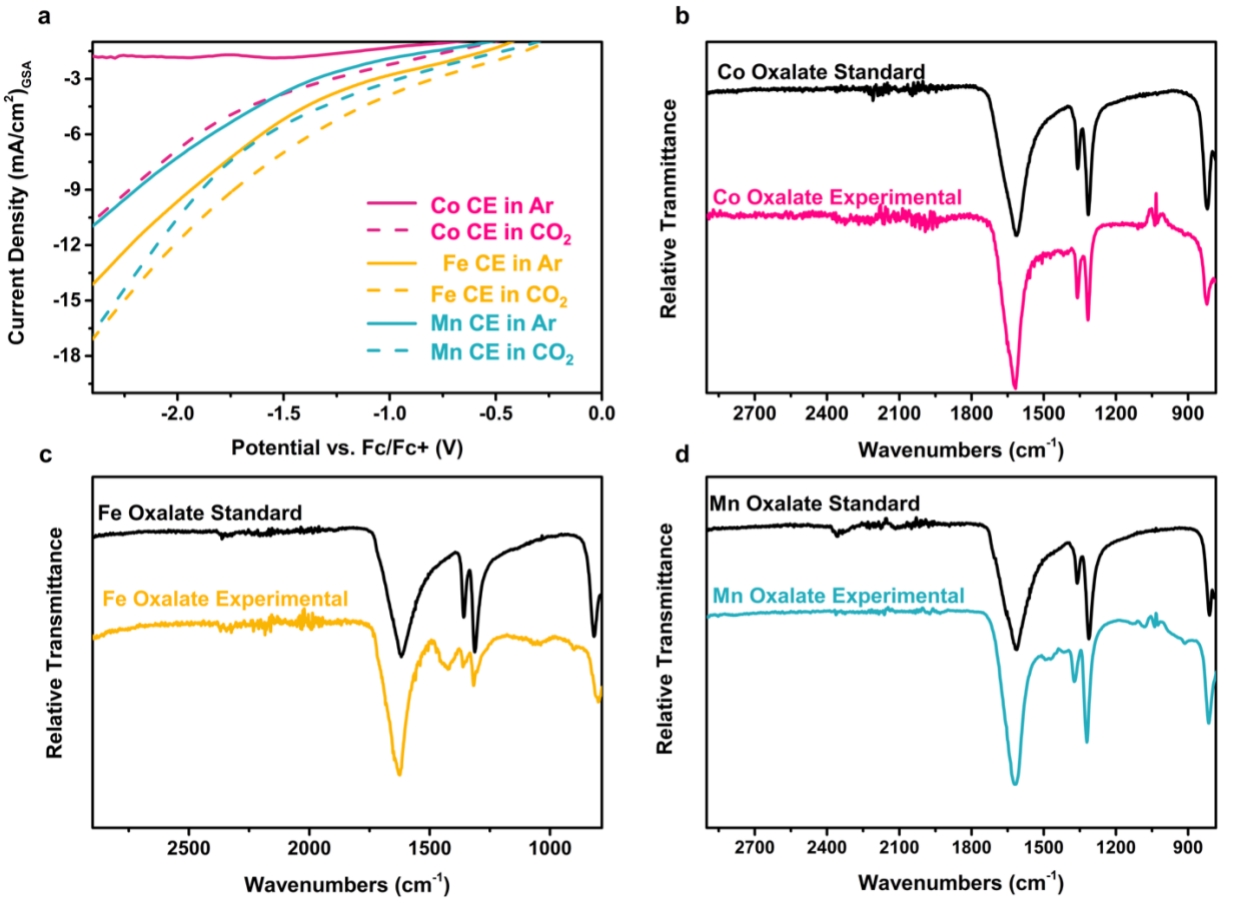


Figure S10. LSVs of TP-PTFE with different anodes (a) under Ar and CO_2 streams. Representative ATR-FTIR spectra of solid products from CO_2R electrolysis at −1.9 V vs Fc/Fc^+ at (b) CoC_2O_4, (c) FeC_2O_4, and (d) MnC_2O_4. The solid precipitates from the electrolyses show characteristic oxalate peaks consistent with C_2O_4: C=O asymmetrical stretch (1625 cm^{-1}), C-O symmetrical stretch (1375 cm^{-1}), and O=C-O angular deformation (1325 cm^{-1}).

Table S7. Faradaic efficiency values for TP-PTFE with different SAs

Potential	**CoC_2O_4**	**CO**	**H_2**
-2.2	70.6 ± 15.0	13.0 ± 10.3	1.3 ± 1.1
-2.1	79.3 ± 3.5	5.4 ± 4.9	1.3 ± 1.3
-2.0	81.8 ± 7.6	7.3 ± 6.2	1.0 ± 1.8
-1.9	83.0 ± 8.0	6.9 ± 3.5	4.5 ± 1.4
Potential	**FeC_2O_4**	**CO**	**H_2**
-2.2	80.1 ± 6.3	2.4 ± 3.2	3.3 ± 2.2
-2.1	85.1 ± 4.1	1.3 ± 0.7	4.5 ± 3.5
-2.0	75.5 ± 10.9	15.4 ± 14.7	1.0 ± 0.9
-1.9	85.8 ± 1.1	7.8 ± 5.7	4.6 ± 3.2
Potential	**MnC_2O_4**	**CO**	**H_2**
-2.2	78.4 ± 12.6	3.8 ± 2.4	3.2 ± 2.3
-2.1	75.1 ± 3.7	9.6 ± 10.1	3.7 ± 1.9
-2.0	76.4 ± 10.6	4.5 ± 5.88	3.7 ± 2.7
-1.9	83.8 ± 2.2	3.9 ± 3.7	11.8 ± 4.4

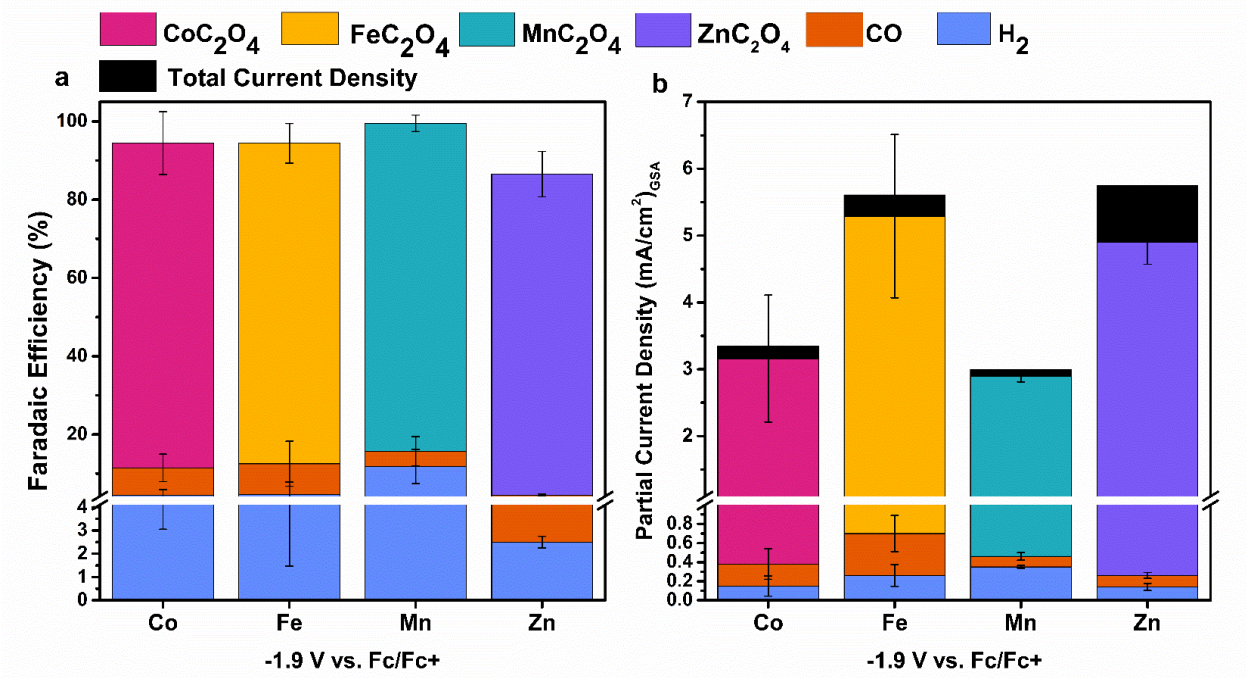


Figure S11. Product distribution (a) and partial current density (b) for Co, Fe, Mn, and Zn counter electrodes.

Characterization of Metal Oxalates

XRD

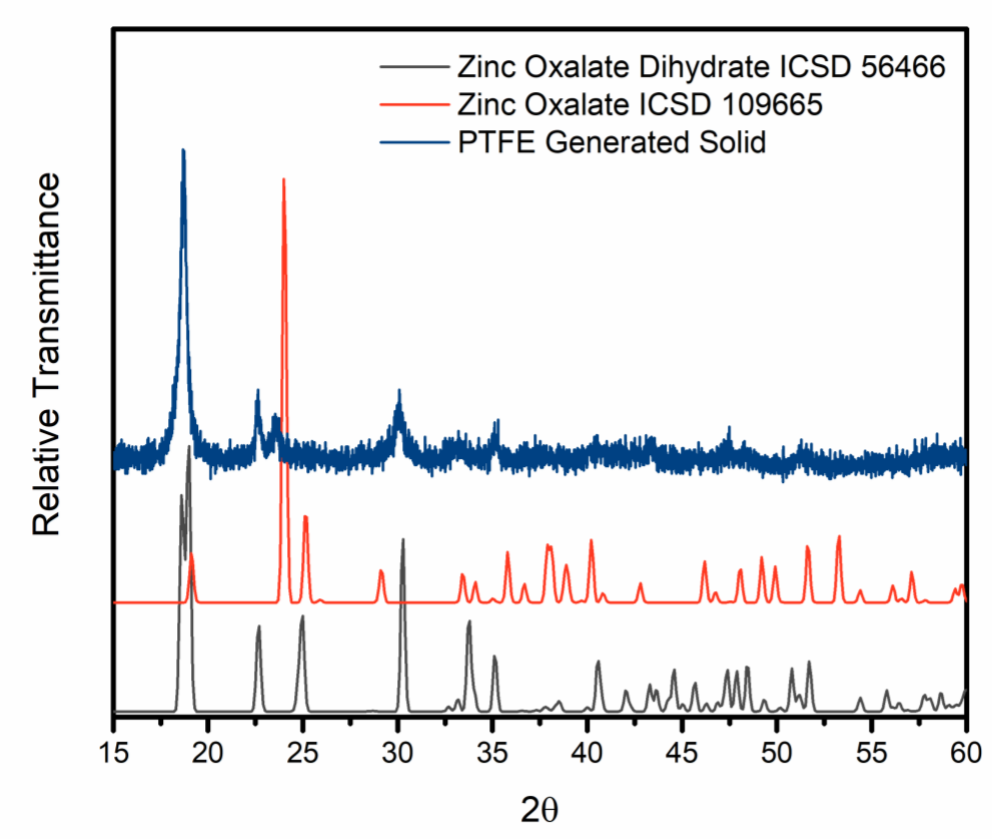


Figure S12. XRD pattern overlaid with published patterns for ZnC_2O_4 *$2H_2O$ and ZnC_2O_4.

PXRD of Co, Fe, and Mn oxalate

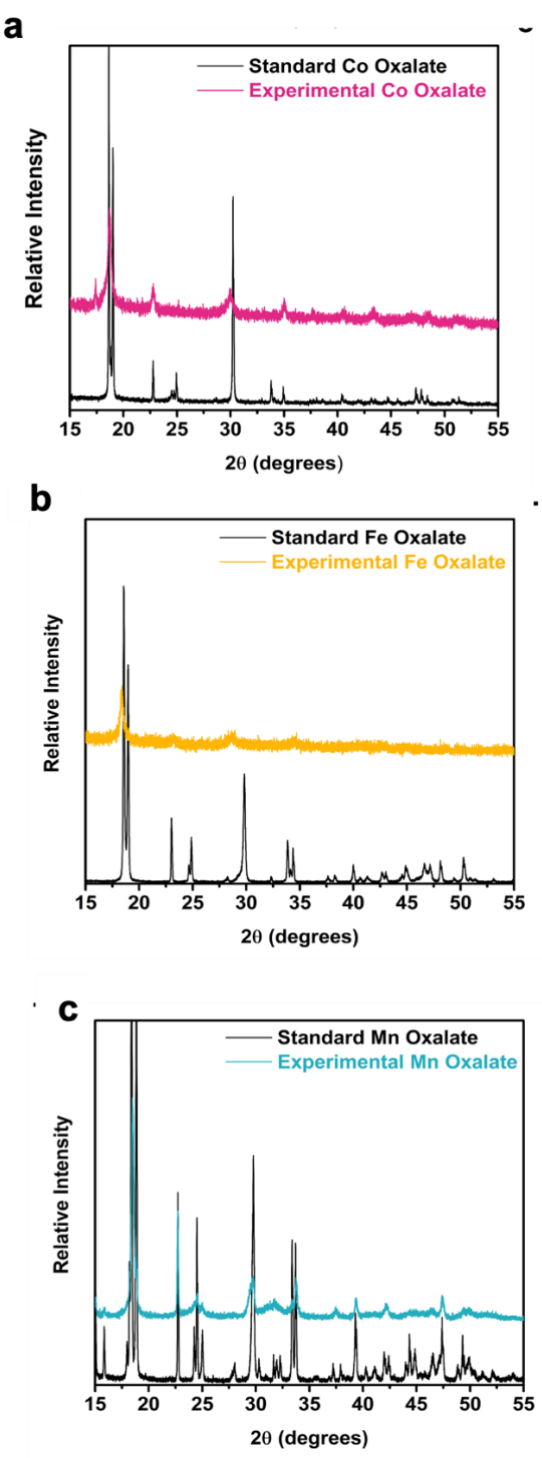


Figure S13. XRD pattern of experimental solids overlaid with standards of CoC_2O_4 (a), FeC_2O_4 (b), and MnC_2O_4 (c).

XPS of Experimental Zinc Oxalate vs. Standard Zinc Oxalate

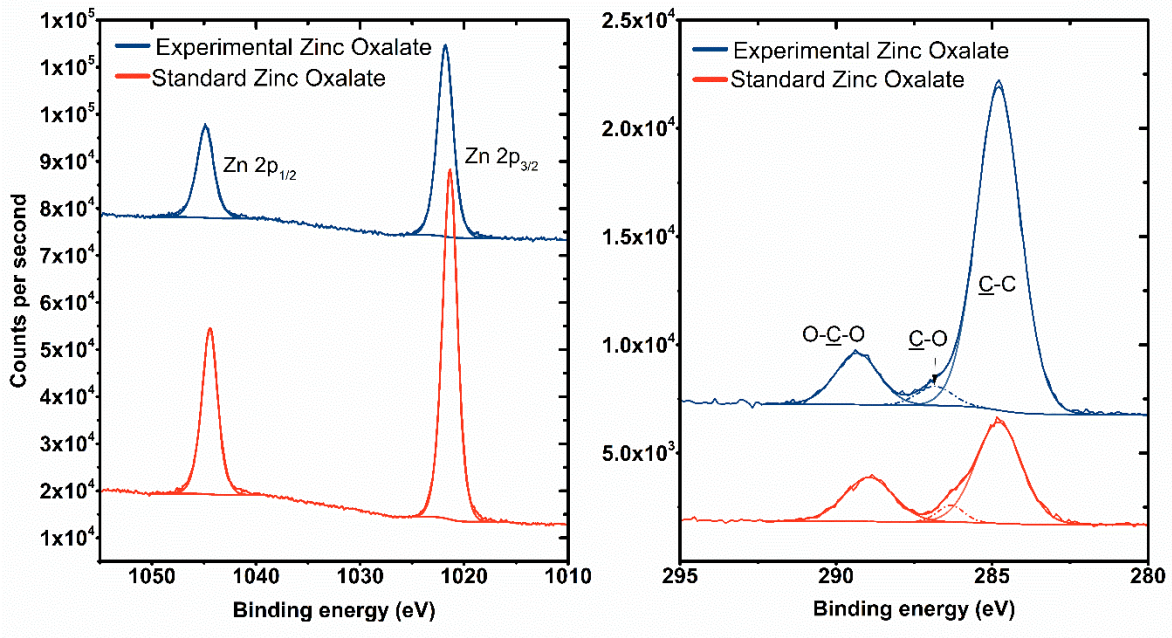


Figure S14. XPS spectrum of Zn 2p region (left) and XPS spectrum of C 1s spectrum (right).

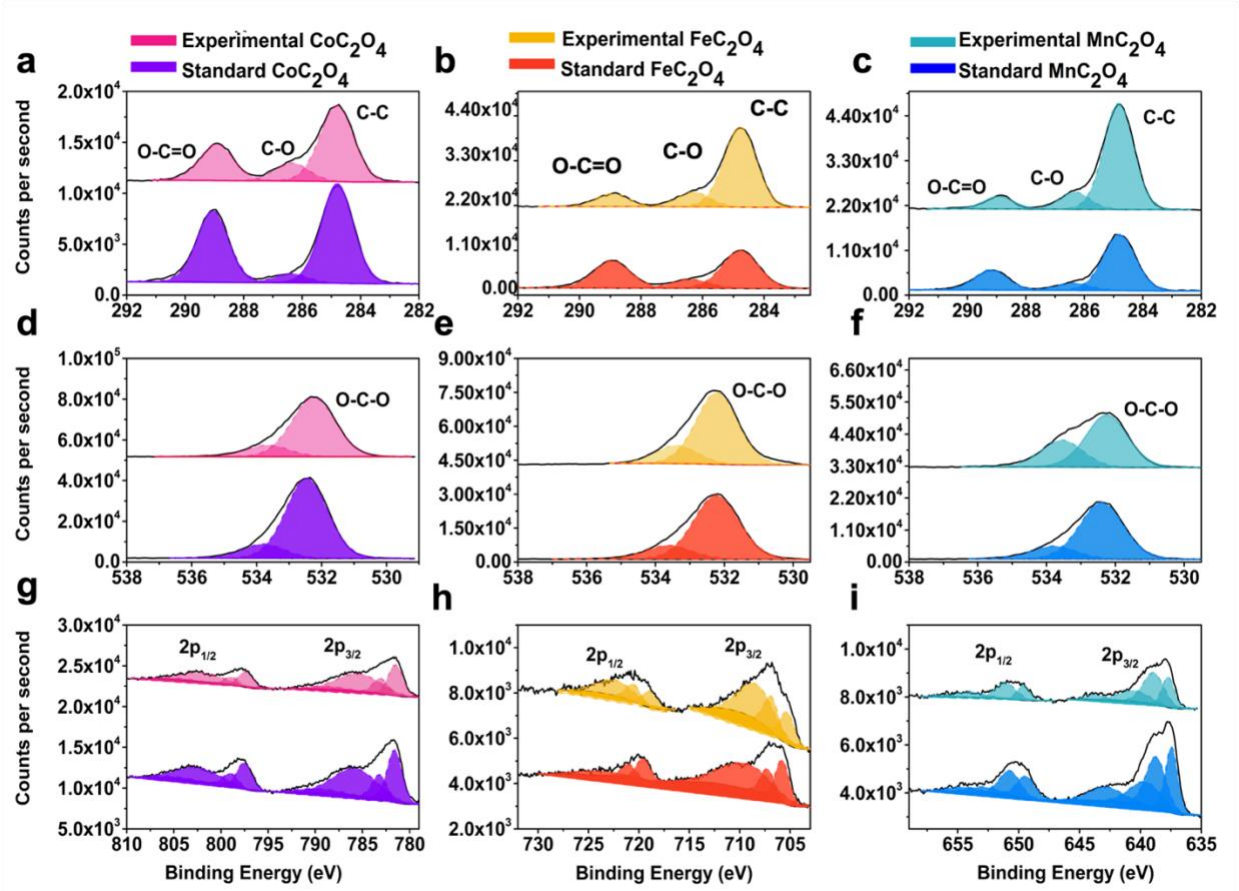


Figure S15. XPS spectra of C 1s region of CoC_2O_4 (a), FeC_2O_4 (b), and MnC_2O_4 (c), O 1s region of CoC_2O_4 (d), FeC_2O_4 (e), and MnC_2O_4 (f), and Co 2p of CoC_2O_4 (g), Fe 2p of FeC_2O_4 (h), and Mn 2 p of MnC_2O_4 (i).

Characterization of Electrode Surface

XRD

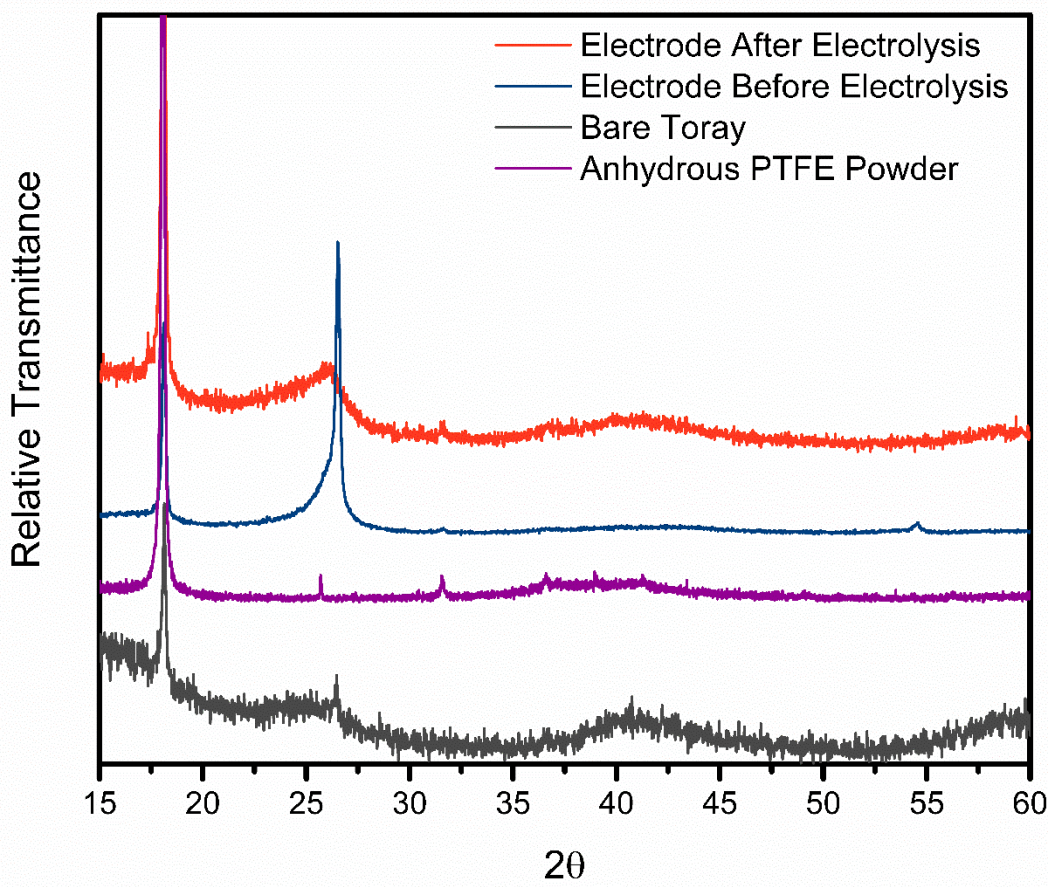


Figure S16. X-ray diffractogram of electrodes before and after electrolysis compared to bare toray paper and anhydrous ptfe powder.

CP-PTFE Pre and Post Electrolysis

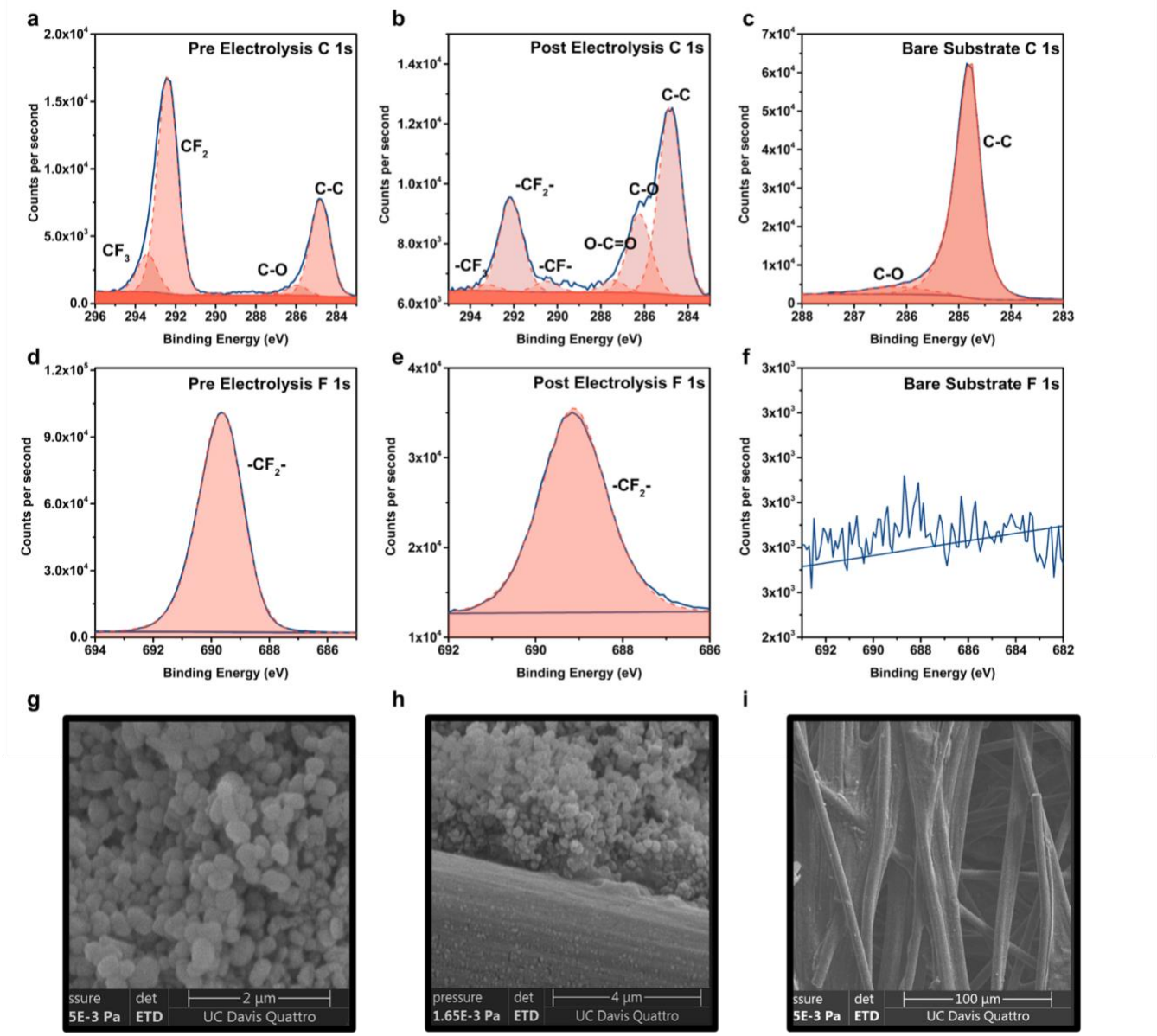


Figure S17. Postmortem characterization of the CP-PTFE (a-c) Representative high resolution XPS spectra in the C 1s region of (a) as-preparedCP-PTFE, (b) CP-PTFE post-electrolysis, and (c) the underlying CP electrode. (d-f) Representative high resolution XPS spectra in the F 1s region of (d) as-prepared TP-PTFE, (e) TP-PTFE post-electrolysis, and (f) the underlying TP electrode. (g-i) Representative SEM micrographs of (g) as-prepared TP-PTFE, (h) TP-PTFE post-electrolysis, and (i) the underlying TP electrode.

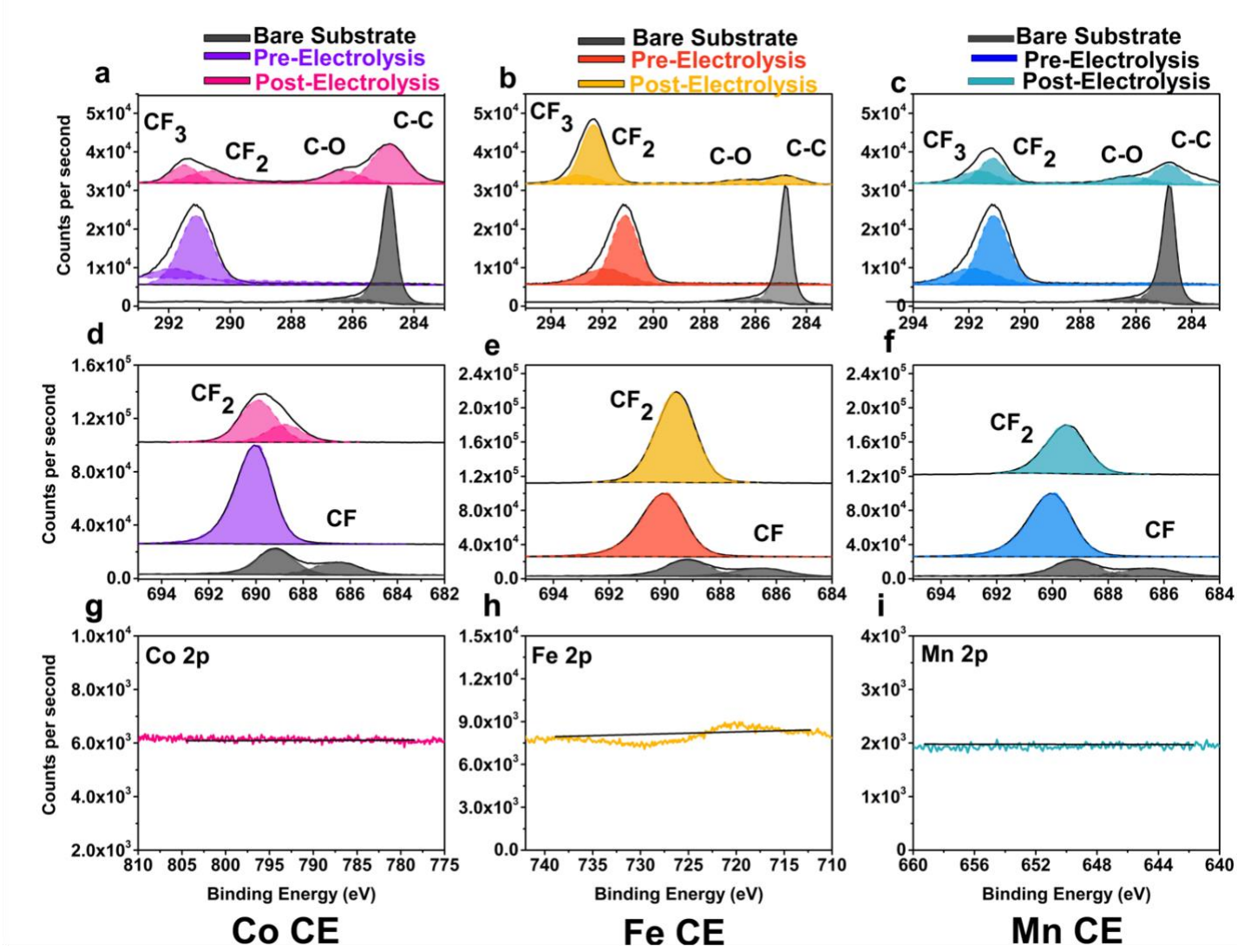


Figure S18. XPS analysis of TP-PTFE electrodes pre and post electrolysis with each respective sacrificial anode for the C 1s region a-c, the F 1s region d-f, and the 2p region g-i.

Table S8. ICP-MS amounts of Pb on TP and TP-PTFE Pre and Post Electrolysis

Electrodes	Pre-Electrolysis	Post-Electrolysis
TP	7.9 ± 2.2	7.6 ± 2.0
TP-PTFE	6.4 ± 1.6	5.6 ± 1.8

EDS

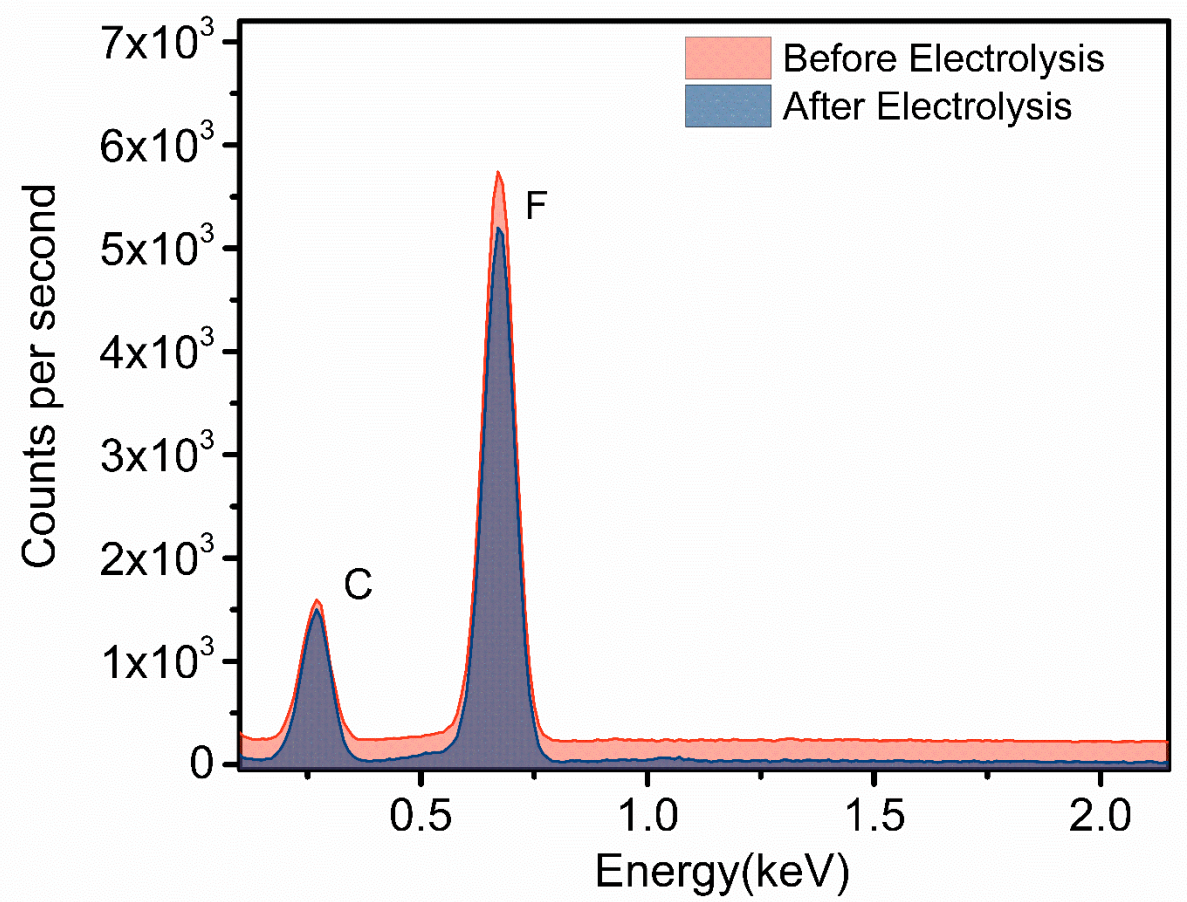


Figure S19. EDS before and after electrolysis of the electrode surface.

Isotopic Labeling with ATR-FTIR and MALDI

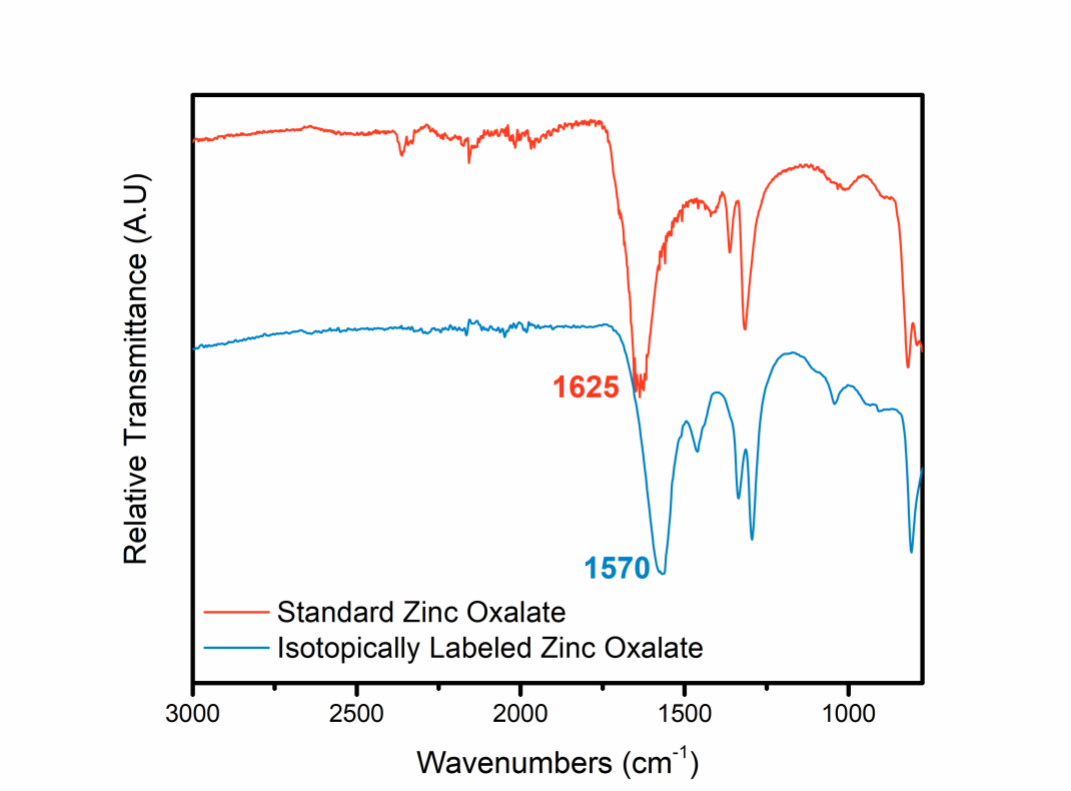


Figure S20. FTIR spectrum of our experimentally generated $Zn^{13}C_2O_4$ as a product of the CPE experiments under $^{13}CO_2$ oxalate compared to a commercial unlabeled ZnC_2O_4 standard.

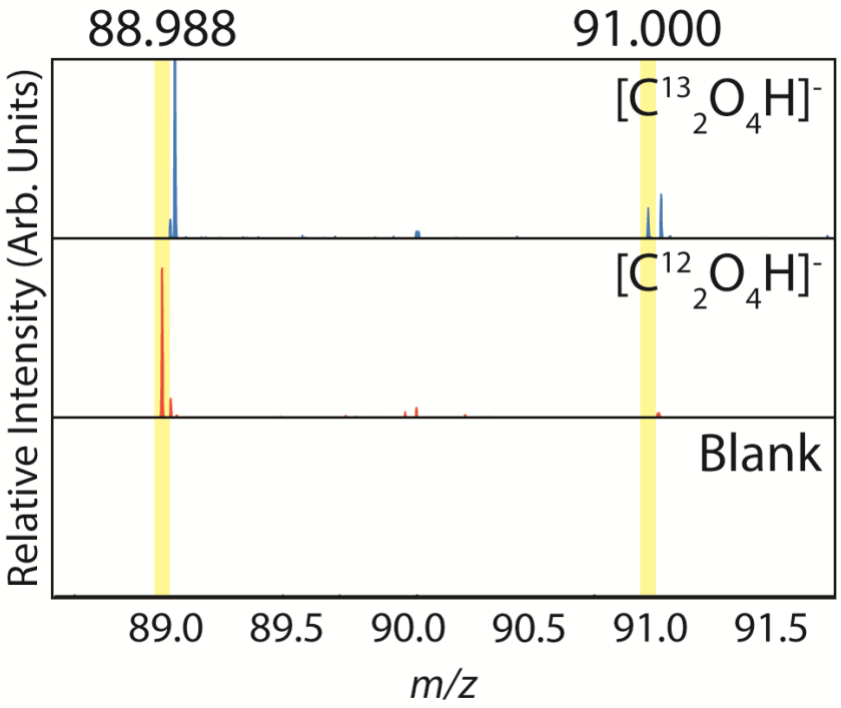


Figure S21. Mass spectra displaying ions associated with isotopically labeled oxalate ion (top), the nonlabelled oxalate ion (middle), and the blank (bottom). The two dalton shift between the isotopically labelled and the unlabeled oxalate ion is consistent with the presence of two C^{13}.

Anhydrous Solvent

Propylene Carbonate purchased from Sigma Aldrich was used as the anhydrous solvent.

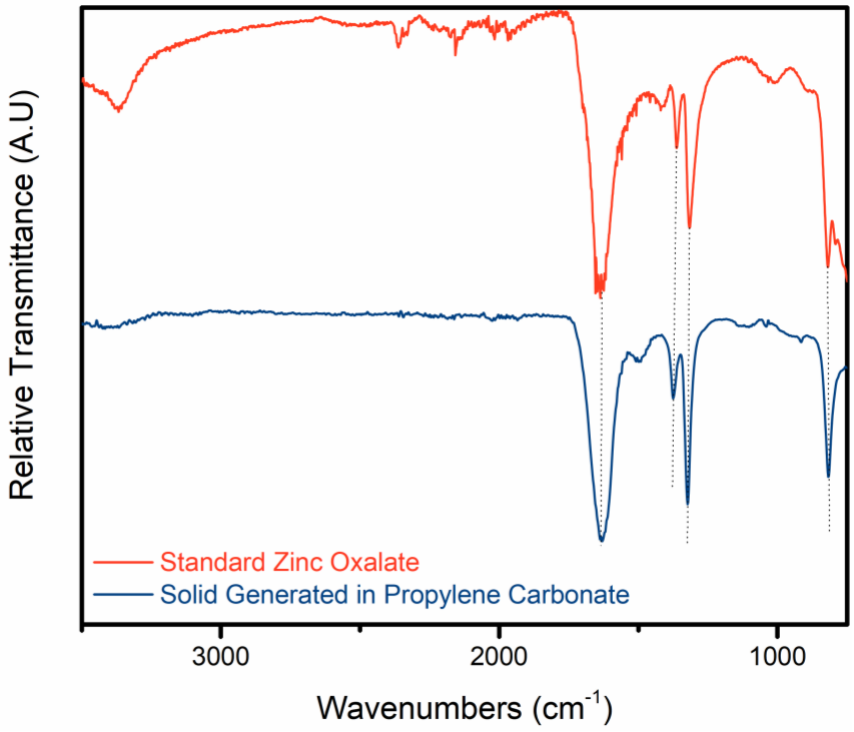


Figure S22. FTIR of the solid generated in propylene carbonate overlaid with a zinc oxalate standard.

Supporting Electrolyte
Tetrapropyl ammonium perchlorate purchased from Sigma Aldrich was used as a supporting electrolyte.

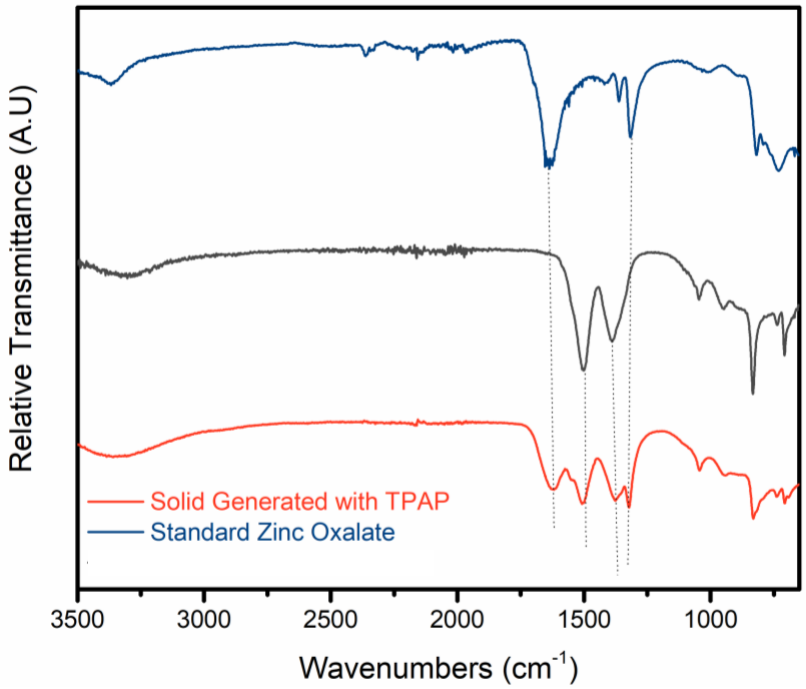


Figure S23. FTIR of solid generated with anhy. PTFE with Tetrapropylammonium perchlorate as a supporting electrolyte under CO_2.

Type of polymer

A polyvinylidene dispersion purchased from Sigma Aldrich was used as a polymer source.

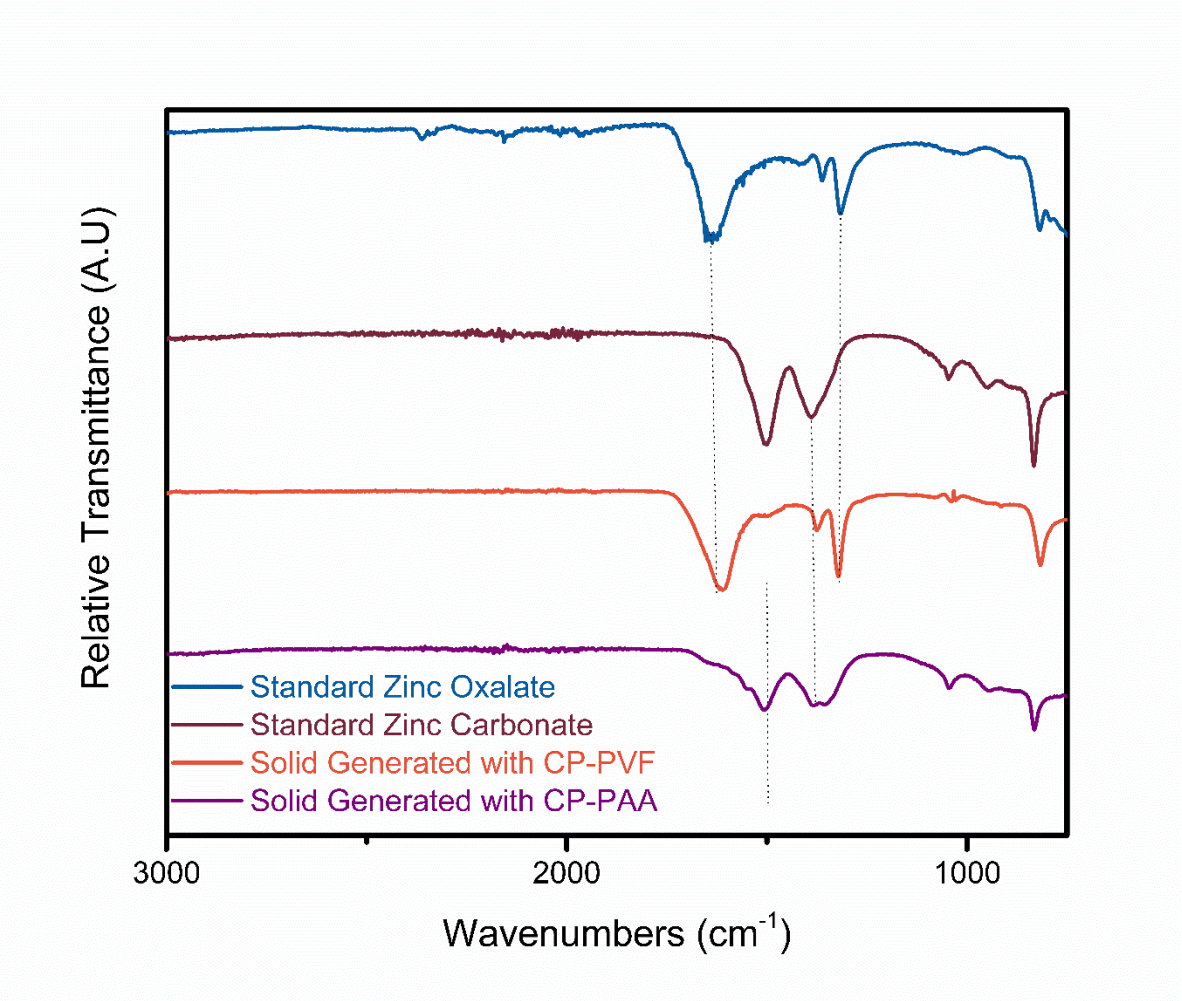


Figure S24. FTIR of the solid generated using polyvinylidene dispersion overlaid with a zinc oxalate standard.

Cell over Time with Zn Counter Electrode

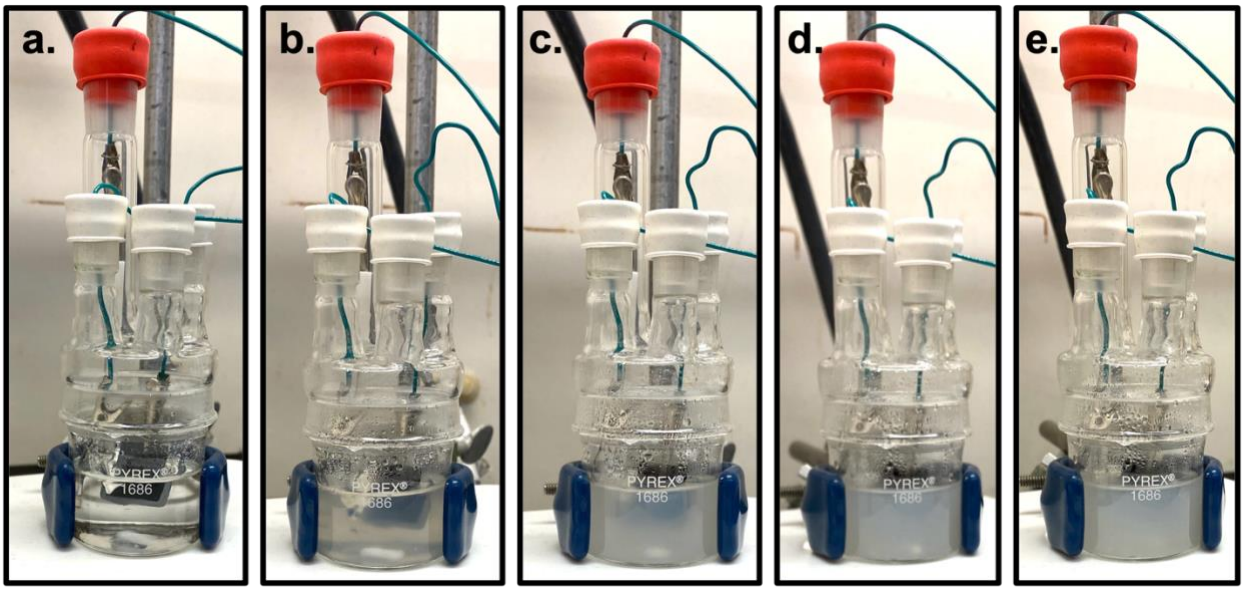


Figure S25. A cell after 0 Coulombs (a.), 25 Coulombs (b.), 50 Coulombs (c.), 75 Coulombs (d.), and 100 Coulombs (e.) have passed at negative 2.8 V vs. Ag/AgCl.

References

(1) Gagne, R. R.; Koval, C. A.; Lisensky, G. C. Ferrocene as an internal standard for electrochemical measurements. *Inorganic Chemistry* **1980**, *19* (9), 2854-2855.
(2) Gritzner, G.; Kůta, J. Recommendations on reporting electrode potentials in nonaqueous solvents: IUPC commission on electrochemistry. *Electrochimica Acta* **1984**, *29* (6), 869-873.